ESI for

AIPE-active cationic Ir(III) complexes for efficient detection of 2,4,6-trinitrophenol and oxygen

Ping He,[a] Yan Chen,[a] Xiao-Na Li,[b] Ying-Ying Yan[a] and Chun Liu*[a]

[a] State Key Laboratory of Fine Chemicals, Frontier Science Center for Smart Materials, School of Chemical Engineering, Dalian University of Technology, Dalian 116024, China. E-mail: cliu@dlut.edu.cn

[b] School of Environmental Science and Technology, Key Laboratory of Industrial Ecology and Environmental Engineering (MOE), Dalian University of Technology, Liaoning 116024, China

Contents

Phosphorescence decay traces of Ir(III) complexes.

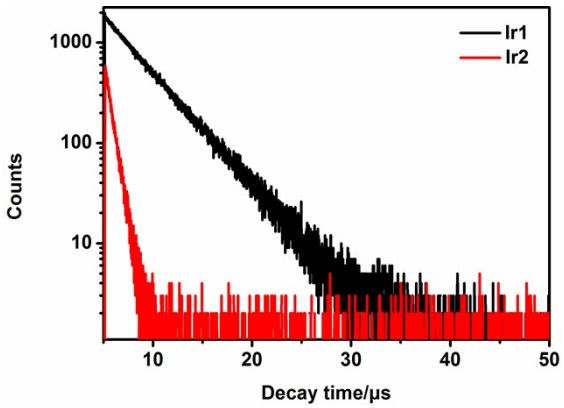

Fig. S1 Phosphorescence decay traces of **Ir1** and **Ir2** in deoxygenated CH_2Cl_2.

Electrochemical properties of Ir(III) complexes.

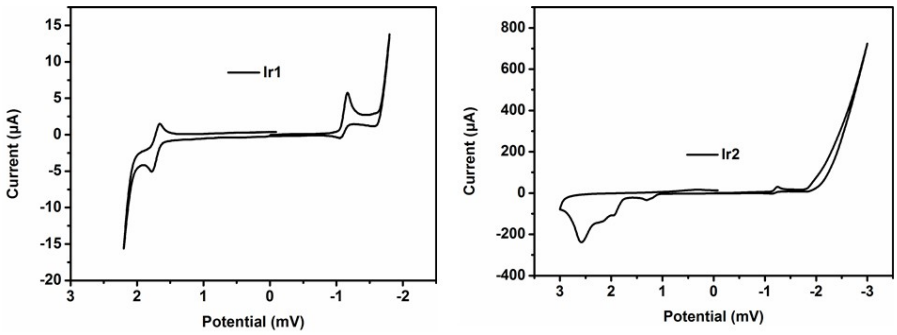

Fig. S2 Cyclic voltammograms of **Ir1**and **Ir2** in deoxygenated CH_2Cl_2 at room temperature.

Luminescence properties of Ir(III) complexes

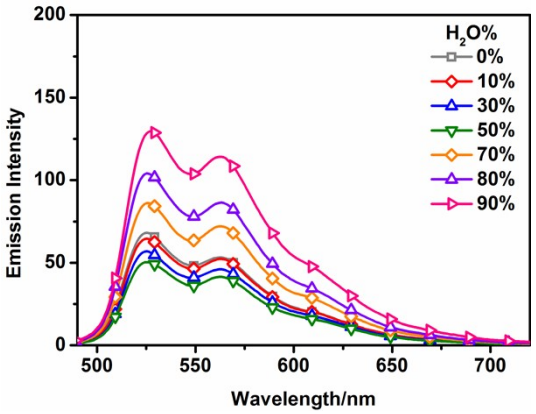

Fig. S3 The emission spectra of complex **Ir1** in H_2O/CH_3CN with different H_2O fractions (0-90% v/v).

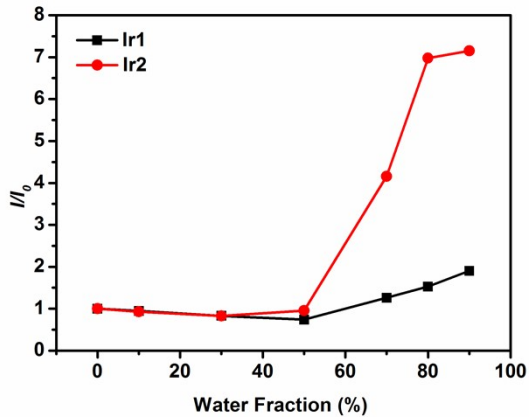

Fig. S4 Plots of relative intensity *vs*. different water fractions for **Ir1** and **Ir2** at the maximum emission wavelength (I_0 represents the emission intensity of the complex in MeCN, I represents the emission intensity under corresponding content of water).

Crystal information for Ir2.

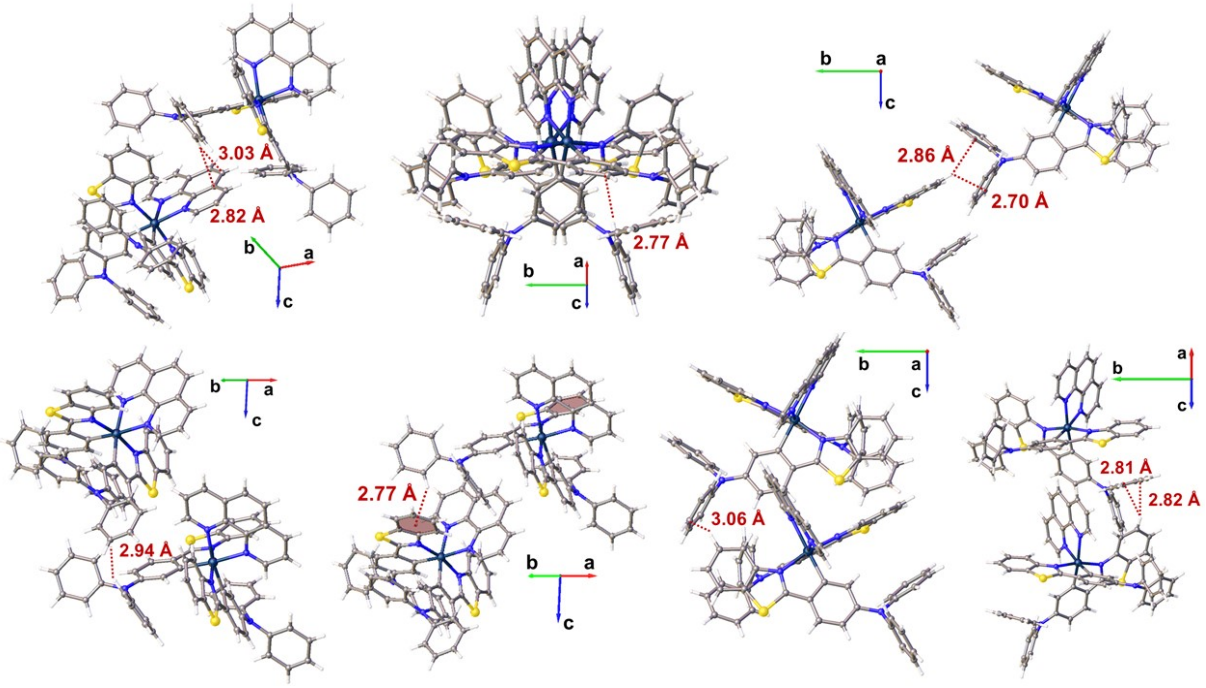

Fig. S5 The C-H···π intermolecular interactions of **Ir2** in the single crystal.

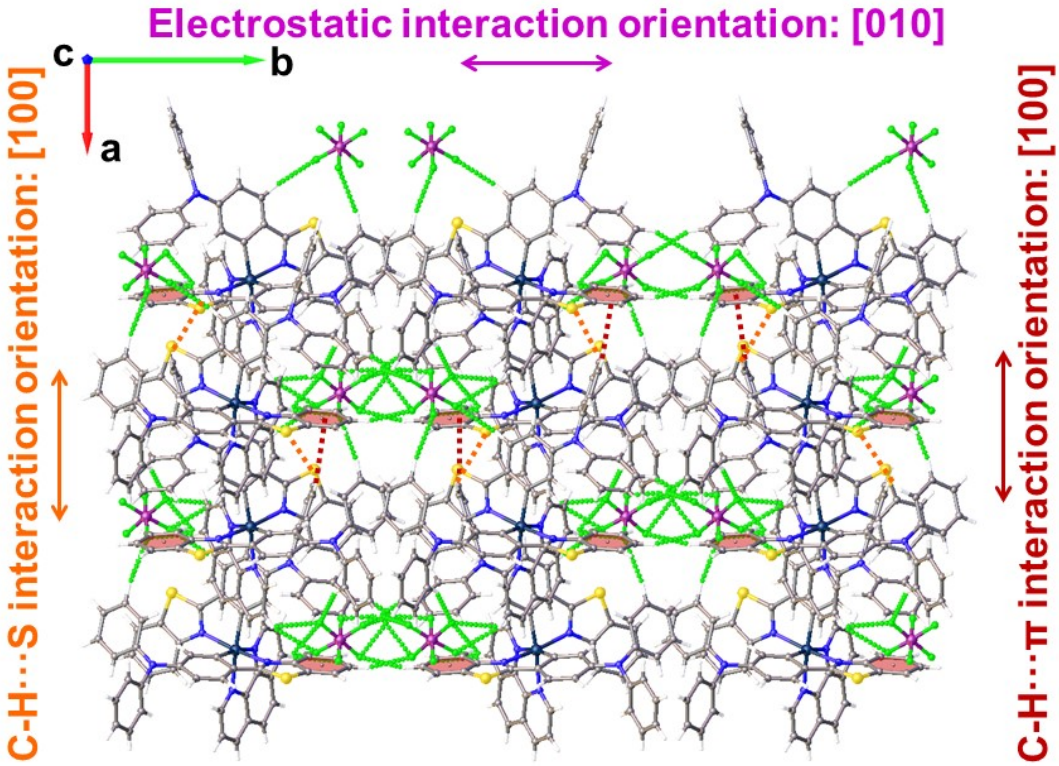

Fig. S6 The molecular stacking of **Ir2** in crystal state (orange dashed lines: C-H···S hydrogen bonds; wine red dashed lines: C-H···π intermolecular interactions; green dashed lines: C-H···F intermolecular interactions.

Tab. **S1** Crystal data of **Ir2**.

Complex	**Ir2**
Formula	$C_{62}H_{42}F_6IrN_6PS_2$
Formula weight	1272.30
Crystal system	Monoclinic
Temperature	200 K
Space Group	Cc
Cell Lengths (Å)	a = 12.5282(6)
	b = 29.0665(14)
	c = 15.1236(8)
Cell Angles (°)	α = 90
	β = 92.8930(17)
	γ = 90
Cell Volume (Å^3)	5500.3(5)
Z	4
Density (g/cm^3)	1.536
F (000)	2536.0
hmax, **kmax**, **lmax**	14, 34, 17
Tmin, **Tmax**	0.684, 0.751
Absorption coefficient/mm^{-1}	2.599
R(int)	0.0467
Data/restraints/parameters	9575/2/704
Goodness-of-fit on F^2	1.022
R_1[a] [$I > 2\sigma(I)$]	0.0305
wR_2[b] [$I > 2\sigma(I)$]	0.0630
R_1[a] (all data)	0.0374
wR_2[b] (all data)	0.0645
CCDC	2170691

[a] $R_1 = \sum||F_o| - |F_c|| / \sum|F_o|$

[b] $wR_2 = [\sum w(F_o^2 - F_c^2)^2 / \sum w(F_o^2)^2]^{1/2}$

Tab. **S2** The distances and angles of the C-H···S intermolecular interactions in **Ir2** crystal (see Fig. 2c).

Complex	Type	Distance/Å	Angle/°
Ir2	C-H···S	3.24	127.79

Tab. **S3** The distances of the C-H···π intermolecular interactions in **Ir2** crystal (see Fig. 2c and Fig. S4).

Complex	Type	Distances/Å
Ir2	C-H···π	2.66
		2.70
		2.77
		2.81
		2.82
		2.86
		2.94
		3.03
		3.06

Tab. **S4** The distances and angles of the C-H···F intermolecular interactions in **Ir2** crystal (see Fig. 2d).

Complex	Type	Distance/Å	Angle/°
Ir2	C-H···F	2.54	152.32
		2.60	169.83
		2.88	168.49
		2.68	153.58
		2.73	129.60
		2.90	142.22

Previously reported TNP sensors.

Tab. **S5** Some Ir(III) complexes are used as TNP sensors and their K_{SV}

Ir(III) complex	Solvent	K_{SV}	References
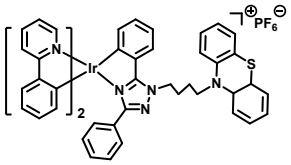	Acetone/H_2O (v/v = 1 : 9)	52800 M^{-1}	[1]
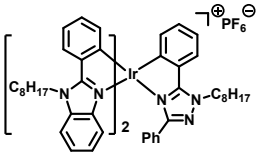	MeCN/H_2O (v/v = 1 : 9)	1600000 M^{-1}	[2]
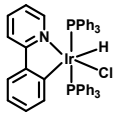	THF/H_2O (v/v = 1 : 9)	190000 M^{-1}	[3]
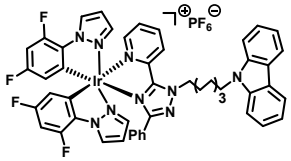	MeCN/H_2O (v/v = 1 : 9)	3790000 M^{-1}	[4]
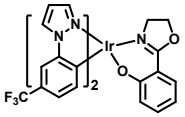	MeCN/H_2O (v/v = 1 : 9)	166000 M^{-1}	[5]
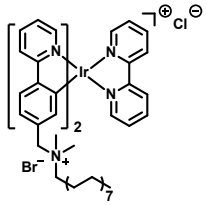	MeCN/H_2O (v/v = 1 : 9)	32200 M^{-1}	[6]
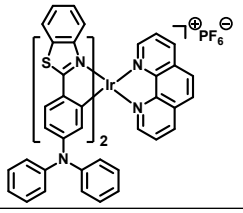	MeCN/H_2O (v/v = 1 : 9)	2644330 M^{-1}	This work

Synthesis of the Ir(III) complex Ir-ppy-dpa for TNP detection

Ir-ppy-dpa was prepared following the reported method (*Mater. Chem. Front.*, 2019, 3, 1593-1600). $IrCl_3 \cdot 3H_2O$ (0.2 mmol, 70.5 mg) and cyclometalating ligand (0.5 mmol, 161.2 mg,) were added in a mixture of 2-ethoxyethanol (6 mL) and water (2 mL). The mixture was then heated to reflux for 24 h under the N_2 atmosphere. After being cooled to room temperature, the solvent was removed in vacuum and the crude product was used for the next step without purification. The dimeric Ir(III) complex reacted with 3.0 equiv. of the 1,10-phenanthroline (0.6 mmol, 108.1 mg) in 2-ethoxyethanol at 120℃ under nitrogen for 24 h. After cooling to room temperature, a 10-fold excess of saturated KPF_6 solution was added and stirred for 2 h. The reaction mixture was added to water (15 mL) and extracted with dichloromethane. The product was isolated by column chromatography.

Ir-ppy-dpa. ^{1}H NMR (400 MHz, DMSO-d_6): δ 8.89 (dd, J = 8.2, 1.2 Hz, 2H), 8.42 - 8.32 (m, 4H), 8.13 (dd, J = 8.2, 5.1 Hz, 2H), 7.80 (d, J = 8.3 Hz, 2H), 7.72 (d, J = 8.7 Hz, 2H), 7.49 - 7.42 (m, 2H), 7.25 (t, J = 7.9 Hz, 8H), 7.05 (t, J = 7.4 Hz, 6H), 6.98 (d, J = 7.6 Hz, 8H), 6.55 (dd, J = 8.6, 2.3 Hz, 2H), 6.53 - 6.46 (m, 2H), 5.88 (d, J = 2.3 Hz, 2H).

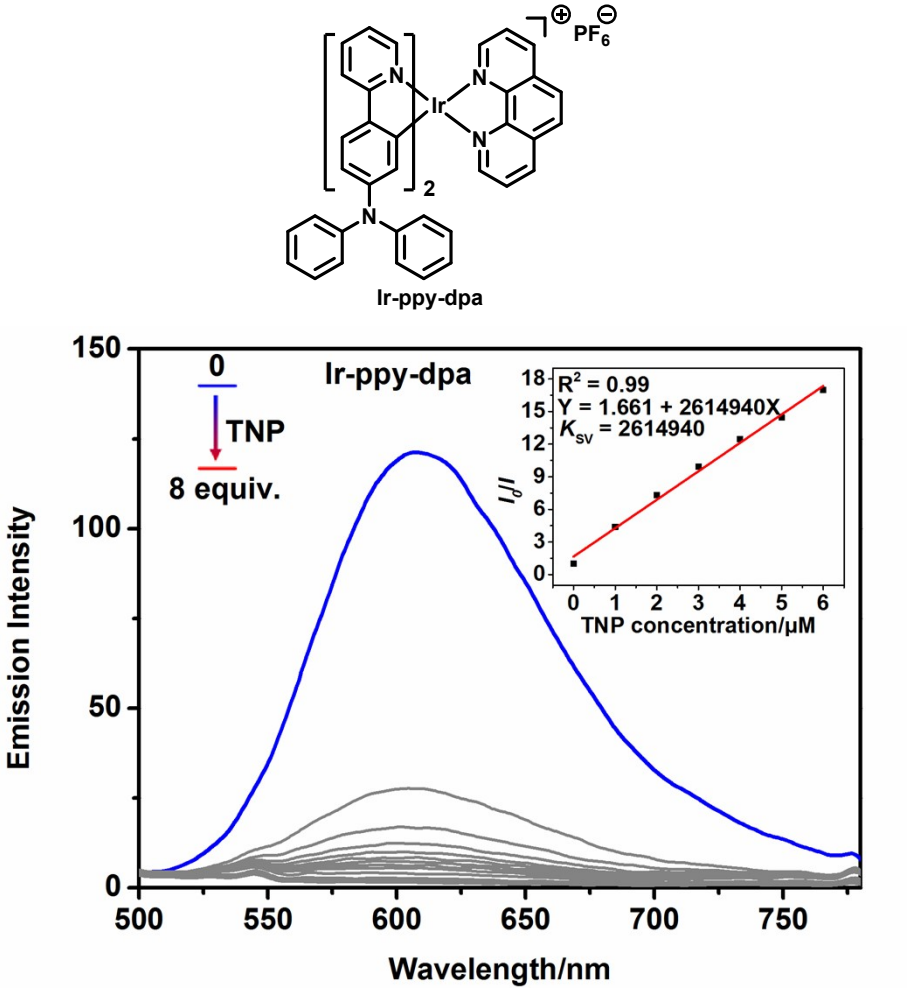

Fig. S7 Structure and emission spectra of **Ir-ppy-dpa** at 10 μM in H_2O/CH_3CN (v/v = 9:1) with

different concentrations of TNP (K_{SV} = 2614940 M^{-1}).

Calculation of detection limits of Ir(III) complexes.

The detection limits of **Ir1**, **Ir2** and **Ir-ppy-dpa** were calculated according to the following equation LOD = 3σ/*K* (σ represents the standard deviation of the blank measurement, *K* represents the slope of the linear regression). The detection limits of **Ir1**, **Ir2** and **Ir-ppy-dpa** for TNP were calculated to be 50.17 nM, 2.23 nM and 19.75 nM, respectively.

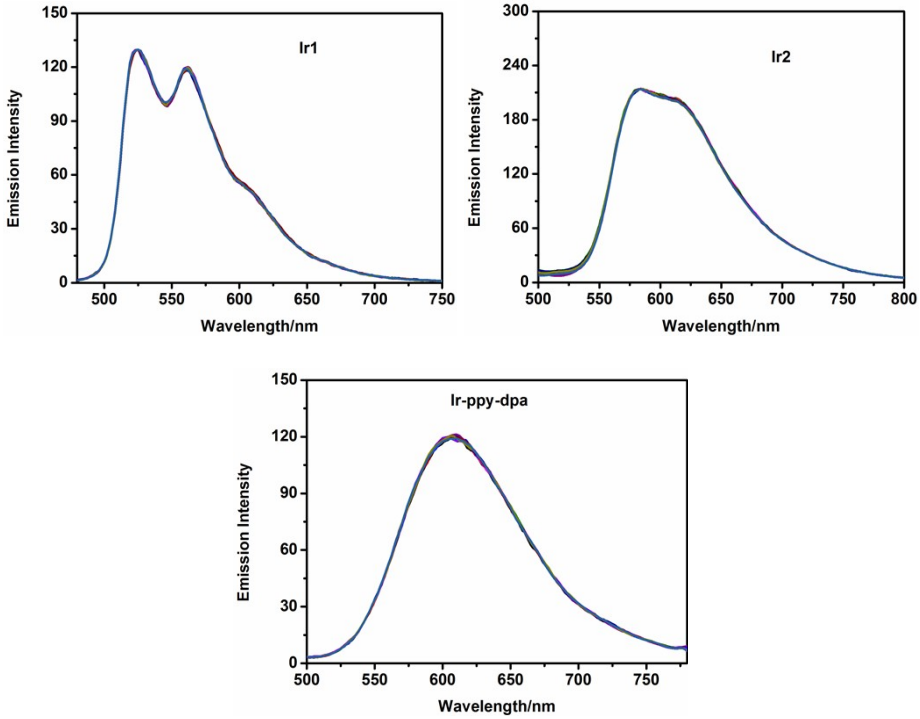

Fig. S8 The blank measurements of **Ir1**, **Ir2** and **Ir-ppy-dpa** for eleven times in H_2O/CH_3CN (v/v = 9:1, 10 μM).

Tab. **S6** The emission intensity of **Ir1** at 525 nm, **Ir2** at 583 nm and **Ir-ppy-dpa** 607 nm in eleven times in H_2O/CH_3CN (v/v = 9:1, 10 μM)

Complexes	X_1	X_2	X_3	X_4	X_5	X_6	X_7	X_8	X_9	X_{10}	X_{11}	X
Ir1	129.69	129.49	129.44	129.68	129.57	129.65	129.71	129.44	129.70	129.62	129.73	129.61
Ir2	213.94	213.89	214.00	213.92	213.92	213.97	213.76	213.67	213.93	213.64	213.73	213.85
Ir-ppy-dpa	120.65	120.52	120.16	120.12	120.03	119.59	119.92	119.19	119.15	119.09	118.94	119.76

The values of σ for **Ir1**, **Ir2** and **Ir-ppy-dpa** were calculated according to the following equation:

$$\sigma = [\sum(X_i\text{-}X)^2/(n\text{-}1)]^{0.5}$$

X_i (i = 1, 2, 3…11) represents the emission intensity of each test, X represents the mean value of the emission intensity, n represents the number of tests.

According to the above formula, the values of σ for **Ir1**, **Ir2** and **Ir-ppy-dpa** were calculated to be 0.1092, 0.1272 and 0.6004, respectively.

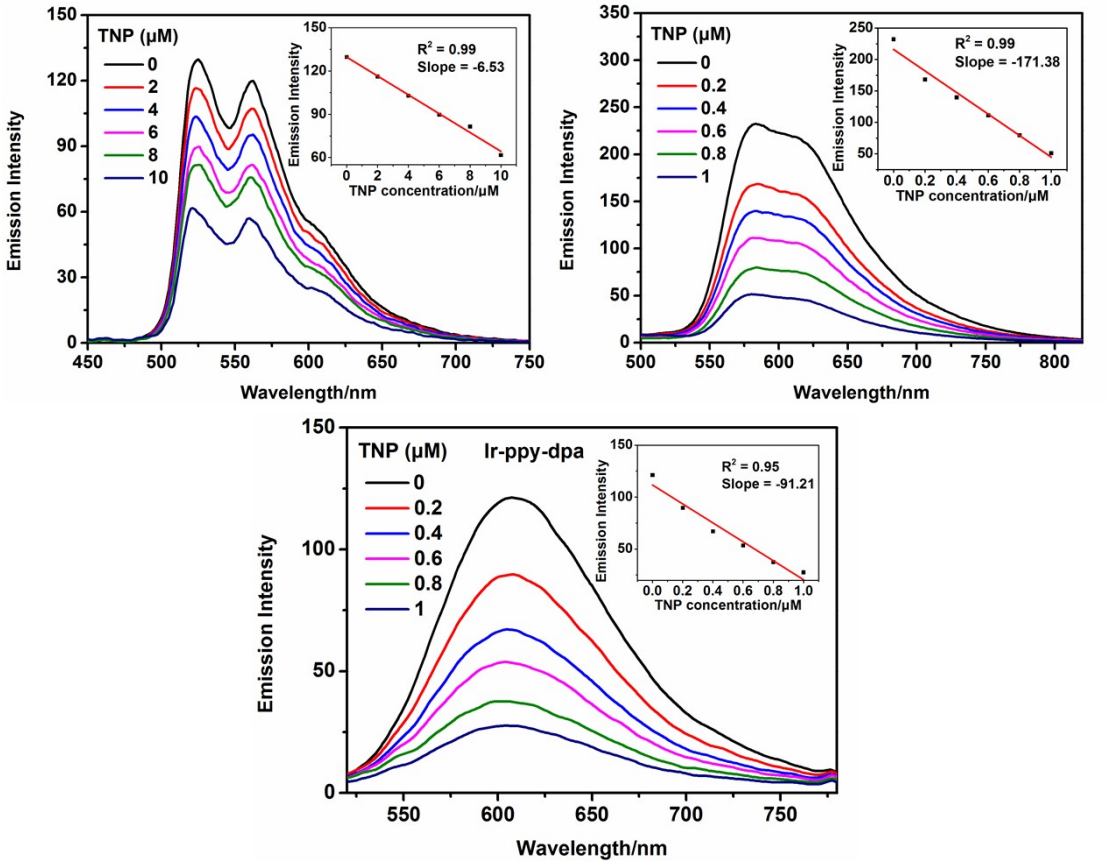

Fig. S9 The emission spectra of **Ir1**, **Ir2** and **Ir-ppy-dpa** at 10 μM in H_2O/CH_3CN (v/v = 9:1) with different concentrations of TNP. Insert: the slope of the linear regression.

HRMS analysis.

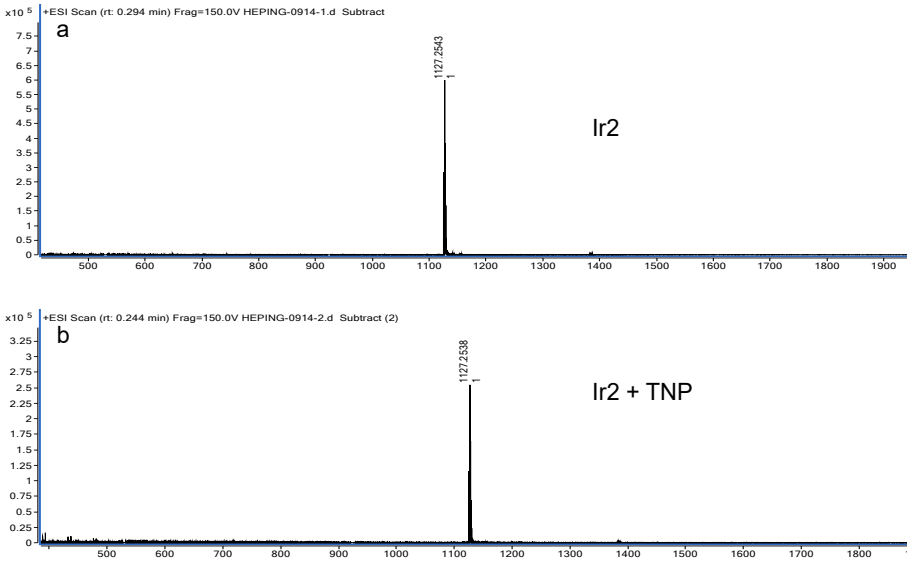

Fig. S10 HRMS of the cationic portion of **Ir2** before (a) and after (b) addition of TNP.

Previously reported OSPs.

Tab. **S7** Some Ir(III) complexes used as oxygen-sensitive probes and their oxygen sensitivity

OSP	Matrix	I_0/I_{100}	References
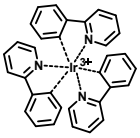	poly(styrene-*co*-TFEM)	15.3	[7]
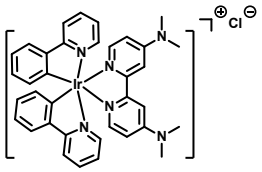	Polystyrene	2.4	[8]
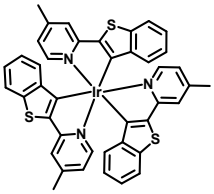	FIB	7.4	[9]
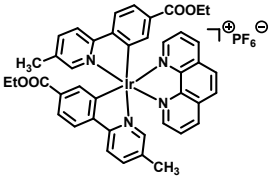	Ethyl cellulose	7.3	[10]
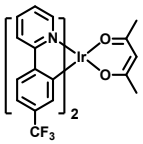	Ethyl cellulose	5.8	[11]
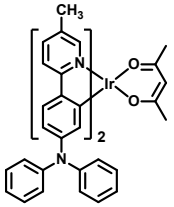	Ethyl cellulose	16.4	[12]
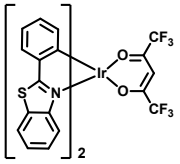	Polystyrene	12.9	[13]
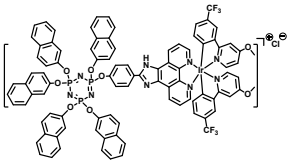	Ethyl cellulose	6.2	[14]
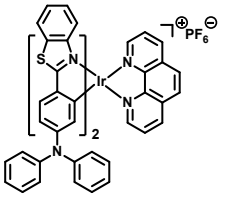	Ethyl cellulose	25.4	This work

References

[1] X. Hou, Y. Wu, H. Cao, H. Sun, H. Li, G. Shan and Z. Su, *Chem*. *Commun*., 2014, **50**, 6031-6034.

[2] Y. Han, H. Cao, H. Sun, G. Shan, Y. Wu, Z. Su and Y. Liao, *J. Mater. Chem. C,* 2015, **3**, 2341-2349.

[3] P. Alam, G. Kaur, V. Kachwal, A. Gupta, A. Roy Choudhury and I.R. Laskar, *J. Mater*. *Chem*. *C*, 2015, **3**, 5450-5456.

[4] L. Wen, X. Hou, G. Shan, W. Song, S. Zhang, H. Sun and Z. Su, *J. Mater. Chem. C,* 2017, **5**, 10847-10854.

[5] W. Che, G. Li, X. Liu, K. Shao, D. Zhu, Z. Su and M. R. Bryce, *Chem*. *Commun*., 2018, **54**, 1730-1733.

[6] S. Yi, Z. Lu, Z. Xie and L. Hou, *Talanta*, 2020, **208**, 120372.

[7] Y. Amao, Y. Ishikawa and I. Okura, *Anal. Chim. Acta*, 2001, **445**, 177-182.

[8] J.F. Fernández-Sánchez, T. Roth, R. Cannas, M.K. Nazeeruddin, S. Spichiger, M. Graetzel and U.E. Spichiger-Keller, *Talanta*, 2007, **71**, 242-250.

[9] B. Carlson, B.E. Eichinger, W. Kaminsky and G. D. Phelan, *Sens*. *Actuators*, *B*, 2010, **145**, 278-284.

[10] C. Liu, H. Yu, Y. Xing, Z. Gao and Z. Jin, *Dalton Trans*., 2016, **45**, 734-741.

[11] C. Liu, X. Lv, Y. Xing and J. Qiu, *J. Mater. Chem. C*, 2015, **3**, 8010-8017.

[12] C. Liu, H. Yu, X. Rao, X. Lv, Z. Jin and J. Qiu, *Dyes Pigm.*, 2017, **136**, 641-647.

[13] R. Kai, W. Jun and J. Huali, *Sens*. *Actuators*, *B*, 2017, **240**, 697-708.

[14] M. Zeyrek Ongun, M. Sahin, T. Akbal, N. Avsar, H. Karakas, K. Ertekin, D. Atilla, H. İbişoğlu and S.Z. Topal, *Spectrochim*. *Acta*, *Part A*, 2020, **239**, 118490.

The reversibility for sensing oxygen of Ir1.

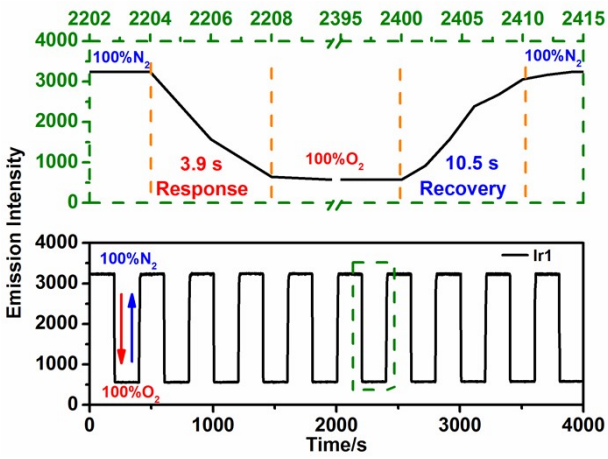

Fig. **S11** Reversibility and emission intensity response of sensing film of **Ir1** immobilized in EC when cycling from 100% N_2 to 100% O_2.

NMR and HRMS spectra of complexes Ir1 and Ir2.

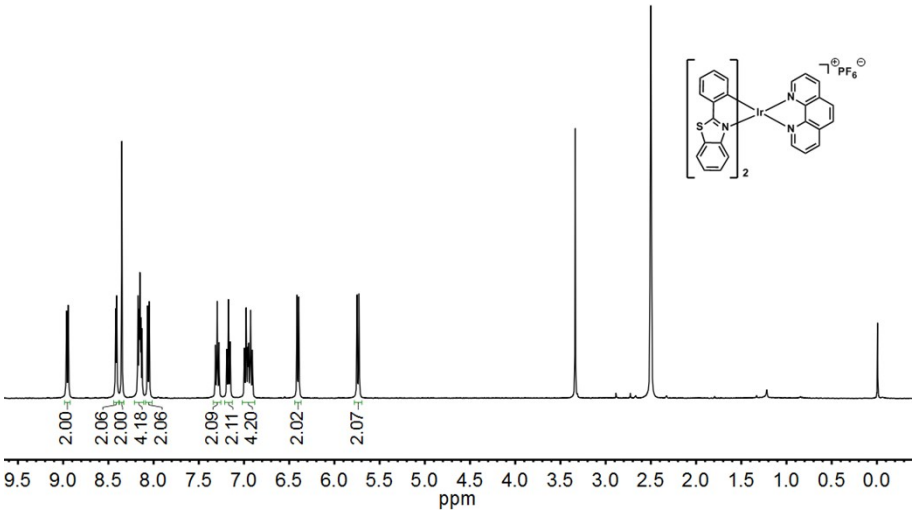

Fig. **S12**. The ^{1}H NMR spectrum of **Ir1** in DMSO-d_6.

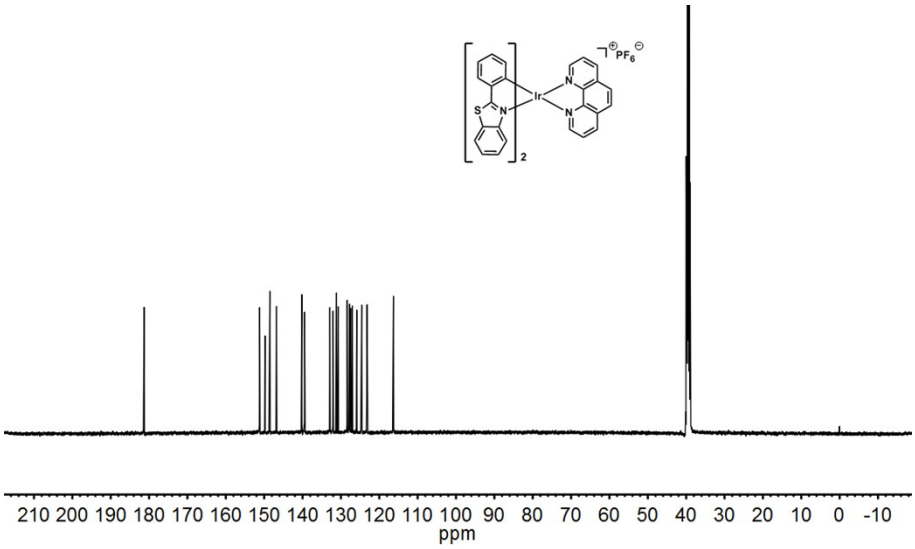

Fig. **S13**. The ^{13}C NMR spectrum of **Ir1** in DMSO-d_6.

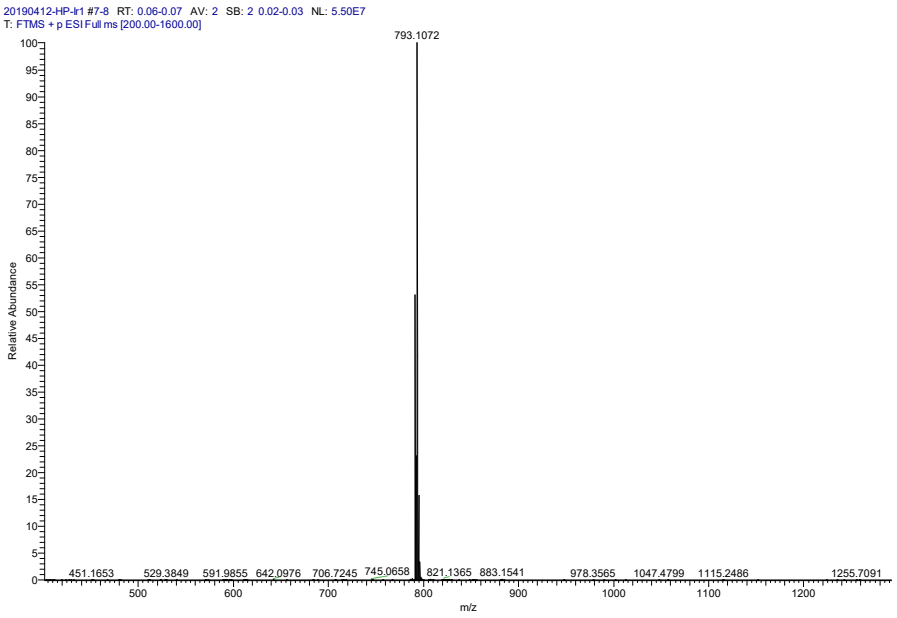

Fig. **S14**. The HRMS spectrum of the cationic portion of **Ir1**.

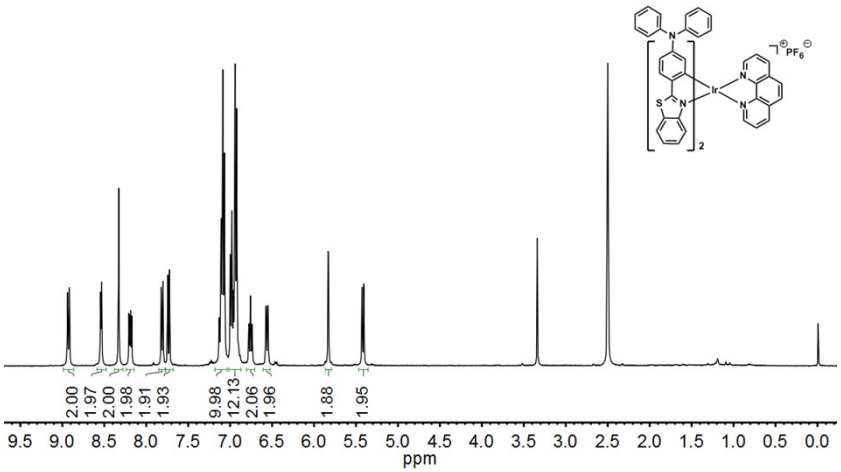

Fig. **S15** ^{1}H NMR spectrum of **Ir2** in DMSO-d_6.

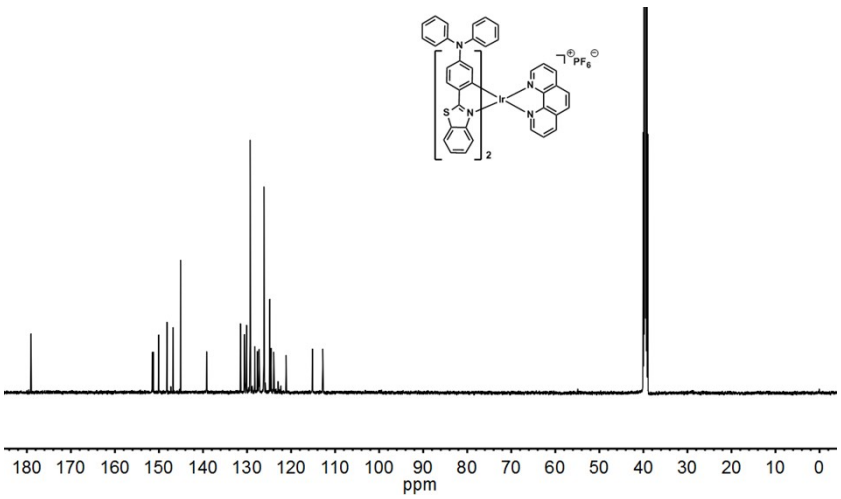

Fig. **S16** ^{13}C NMR spectrum of **Ir2** in DMSO-d_6.

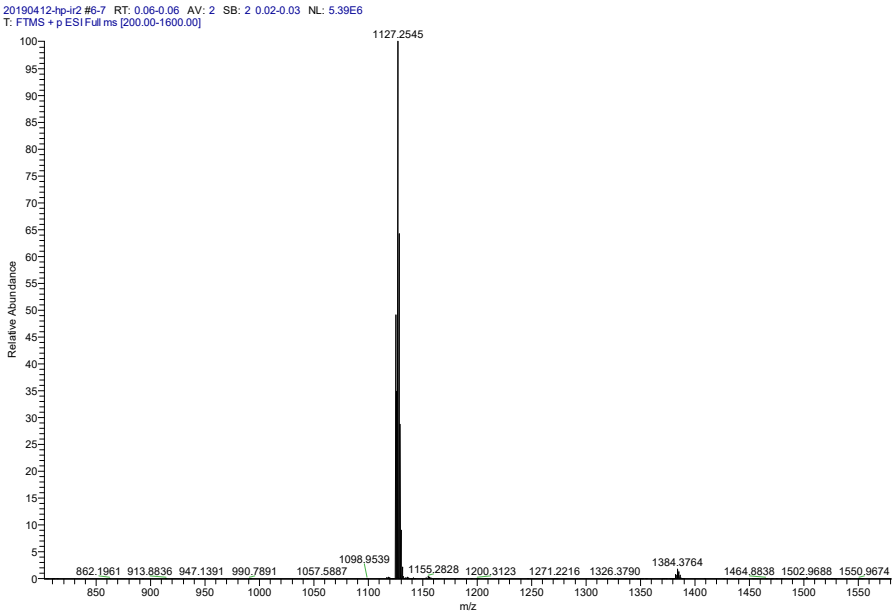

Fig. **S17** The HRMS spectrum of the cationic portion of **Ir2**.